Anal. Chem. **2009,** *81,* 7667–7676

Electrochemical Determination of Flow Velocity Profile in a Microfluidic Channel from Steady-State Currents: Numerical Approach and Optimization of Electrode Layout

Christian Amatore,*,† Oleksiy V. Klymenko,‡ Alexander I. Oleinick,‡ and Irina Svir*,†,‡

Département de Chimie, Ecole Normale Supérieure, UMR CNRS-ENS-UPMC 8640 "PASTEUR", 24 rue Lhomond, 75231 Paris Cedex 05, France, and Mathematical and Computer Modelling Laboratory, Kharkov National University of Radioelectronics, 14 Lenin Avenue, 61166 Kharkov, Ukraine

In this article, the numerical approach for flow profile reconstruction in a microfluidic channel equipped with band microelectrodes introduced previously by the authors, based on transient currents, is extended to the exclusive use of steady-state currents. It is shown that, although the currents obey steady state, the flow velocity profile in the channel may be reconstructed rapidly with a high accuracy, provided a sufficient number of electrodes performing under steady state are considered. The present theory demonstrates how the electrode widths and sizes of gaps separating them can be optimized to achieve better performance of the method. This approach has been evaluated theoretically for band microelectrode arrays embedded into one wall of a rectangular channel consisting of three, four, or five electrodes, all of which are operated in the generator mode. The results prove that the proposed approach is able to accurately recover the shape of the flow profile in a wide range of Peclet numbers and flow types ranging from the classical parabolic Poiseuille flow to constant electro-osmotic-type flow.

The miniaturization of analytical devices has been shown to provide many specific advantages,[1] mostly because (i) the amount of sample required for the analysis is minimized and (ii) the flow velocity profiles of the solution carriers are expected to be better controlled. However, the reduction of the amount of solution makes precise monitoring of the flow an extremely difficult challenge. When this is a critical issue, one must resort to sophisticated methods, most of them generally involving the direct tracking of particles carried by the flow.[2] Such procedures require obviously good optical quality of the material defining the channel in which the flow is monitored and the use of sophisticated algorithms to follow three-dimensional (3D) displacements of particles from a series of frames. Furthermore, one cannot envision a continuous monitoring of the flow while the microfluidic chip is performing its analytical function, so that feedback control of the flow is prevented.

In previous work, we have examined how arrays of microband electrodes placed transversely on the microchannel floor could supply important information about the flow velocity.[3] In a series of attempts, some of us established, theoretically and experimentally, that the average flow velocity could be measured by a pair of microbands performing in generator−collector mode. However, such procedures did not supply any information about the effective flow velocity distribution, and it was assumed that this obeyed a classical parabolic Poiseuille regime. In a second series of works, we established theoretically that not only the average flow velocity but its distribution could be extracted from transient electrochemical currents.[4] A related work involved voltammetry for monitoring transient hydrodynamic flow profiles in microfluidic flow cells.[5] However, despite many attempts in our laboratory and by others, it seems that the accurate monitoring of transient electrochemical chronoamperometric currents is extremely difficult and certainly may not be used in a routine way, because the transient components are altered by capacitive and ohmic phenomena that cannot be controlled with the proper precision. Conversely, steady-state currents can be monitored with an adequate precision without significant experimental difficulties.

* Authors to whom correspondence should be addressed. E-mails: christian.amatore@ens.fr (C.A.); irina.svir@ens.fr (I.S.).

† Département de Chimie, Ecole Normale Supérieure.

‡ Mathematical and Computer Modelling Laboratory, Kharkov National University of Radioelectronics.

(1) (a) Rossier, J. S.; Girault, H. H. *Lab Chip* **2001**, *1*, 153–157. (b) Kan, C.-W.; Fredlake, C. P.; Doherty, E. A. S.; Barron, A. E. *Electrophoresis* **2004**, *25*, 3564–3588. (c) Dayon, L.; Josserand, J.; Girault, H. H. *Phys. Chem. Chem. Phys.* **2005**, *7*, 4054–4060. (d) Ordeig, O.; Godino, N.; Del Campo, J.; Munõz, F. X.; Nikolajeff, F.; Nyholm, L. *Anal. Chem.* **2008**, *80*, 3622–3632.

(2) For recent examples, see:(a) Plecis, A.; Malaquin, L.; Chen, Y. *J. Appl. Phys.* **2008**, *104*, 124909. (b) Boxx, I.; Heeger, C.; Gordon, R.; Bohm, B.; Aigner, M.; Dreizler, A.; Meier, W. *Proc. Combust. Inst.* **2009**, *32*, 905–912. (c) Li, C.-T.; Chang, K.-C.; Wang, M.-R. *Exp. Therm. Fluid Sci.* **2009**, *33*, 527–537. (d) Wu, S.-C. *Exp. Therm. Fluid Sci.* **2009**, *33* (5), 875−882.

(3) (a) Amatore, C.; Belotti, M.; Chen, Y.; Roy, E.; Sella, C.; Thouin, L. *J. Electroanal. Chem.* **2004**, *573*, 333–343. (b) Amatore, C.; Oleinick, A.; Svir, I. *Electrochem. Commun.* **2004**, *6*, 1123–1130. (c) Amatore, C.; Chen, Y.; Sella, C.; Thouin, L. *Houille Blanche* **2006**, *2*, 60–64. (d) Amatore, C.; Sella, C.; Thouin, L. *J. Electroanal. Chem.* **2006**, *593*, 194–202. (e) Amatore, C.; Da Mota, N.; Sella, C.; Thouin, L. *Anal. Chem.* **2007**, *79*, 8502–8510. (f) Amatore, C.; Da Mota, N.; Sella, C.; Thouin, L. *Anal. Chem.* **2008**, *80*, 4976–4985.

(4) (a) Amatore, C.; Oleinick, A.; Klymenko, O. V.; Svir, I. *ChemPhysChem* **2005**, *6*, 1581–1589. (b) Amatore, C.; Klymenko, O. V.; Svir, I. *ChemPhysChem* **2006**, *7*, 482–487. (c) Amatore, C.; Klymenko, O. V.; Oleinick, A.; Svir, I. *ChemPhysChem* **2007**, *8*, 1870–1874. (d) Klymenko, O. V.; Oleinick, A. I.; Amatore, C.; Svir, I. *Electrochim. Acta* **2007**, *53*, 1100–1106.

(5) Thompson, M.; Compton, R. G. *Anal. Chem.* **2007**, *79*, 626–631.

10.1021/ac9010827 CCC: $40.75
Published on Web 08/21/2009

In this work, we wish to establish theoretically that one may rely on a series of steady-state electrochemical currents monitored at an array of microbands to reconstruct the complete flow velocity pattern within microchannels. The principle of the method is based on the fact that, when an electroactive analyte at constant concentration is carried in a microfluidic channel over an array consisting of microband electrodes placed not too far apart, each electrode sequentially probes one horizontal slice of the solution passing in front of it.[3f] Evidently, the thickness of the solution slice detected by each electrode is dependent both on the diffusivity of the analyte and on the convective drive it experiences at different heights within the channel over the vertical path that it needs to follow to reach the electrode. Because the diffusion component can be predicted and determined with a high degree of precision and accuracy, the information contained in the electrochemical current may be deconvoluted numerically, to provide the flow velocity profile. This was the basis of the previous method; however, in this former attempt, we had to rely on the transient components of the current and not only on the steady-state component.[4]

Here, we wish to establish that, provided that (i) enough microbands are considered and (ii) their placement and geometries are adequate, one can rely exclusively on steady-state currents. Furthermore, we wish to establish that the method may be applied using relative values of the sequence of the steady-state currents monitored by the series of microbands. To us, this seems to be an important issue for a real system operating in a microfluidic channel while it is performing other analytical functions. Indeed, several artifacts (e.g., partial decomposition or reaction with other species, adsorption or retention of the analyte by separative stages placed upstream, etc.) may modify the analyte concentration, so it is unknown at the very place where the steady-state currents need to be monitored. Similarly, microfabrication procedures may lead to imperfect electrode geometries, although when these are manufactured simultaneously, it is expected that they keep their relative sizes.

The theoretical validity of the method will be established hereafter upon considering essentially parabolic-type flows, because the operation of electrochemical arrays under high electrical fields required for electro-osmotic flow is not feasible. However, for the sake of completeness, we will consider the optimization of the electrochemical array under both parabolic Poiseuille and electro-osmotic regimes. Furthermore, this will also provide boundaries of any real situations that can be experienced in a microfluidic channel operating under classical analytical conditions, to evaluate the experimental scope of the method.

THEORY

Diffusion-Convection Problem (Direct Problem). Consider a system of N_{el} microband electrodes embedded into the floor of a microfluidic channel of height h with forced flow (see Figure 1). The solution flowing through the channel contains an electroactive species at a concentration c_0 which is reduced (oxidized) at the electrode surfaces under mass-transport-controlled conditions. All electrodes are assumed to operate under the same potential, and, hence, the system may be considered to consist of "generator" electrodes. The band microelectrode array is described by the coordinates of the electrode edges, i.e., by the set of points x_i^l and x_i^r (where $i = 1, ..., N_{el}$), denoting the positions of the left and right edges of ith electrode. Thus, the width of an electrode with index i is determined by $w_i = x_i^r - x_i^l$ (where $i = 1, ..., N_{el}$), whereas the size of the gap between two adjacent electrodes is $g_i = x_{i+1}^l - x_i^r$. Here, we assume that gap g_i follows an electrode with the same index.

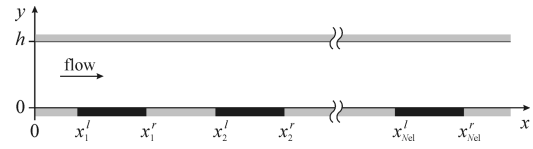

Figure 1. Axial cross section of a microfluidic channel with a band microelectrode array.

We assume that the width of the microchannel is much larger than its height, which is a realistic assumption for most microfluidic applications. Under such conditions, in most parts of the channel, the flow velocity profile $v_x(y)$ is independent of the coordinate z normal to the cross section shown in Figure 1.[6] Hence, the governing equation may be formulated in the given cross section only, thus reducing to the following steady-state two-dimensional diffusion−convection equation:

$$D\left(\frac{\partial^2 c}{\partial x^2} + \frac{\partial^2 c}{\partial y^2}\right) - v_x(y)\frac{\partial c}{\partial x} = 0 \tag{1}$$

where D is the diffusion coefficient of the electroactive species.

Let us introduce the following dimensionless parameters:

$$C = \frac{c}{c_0}$$

$$X = \frac{x}{h}$$

$$Y = \frac{y}{h}$$

$$Pe = \frac{v_{avg}h}{D} \tag{2}$$

where Pe is the Peclet number and v_{avg} is the average flow velocity. Normalized coordinates and lengths will be denoted in the following with the corresponding uppercase symbols.

The dimensionless diffusion−convection equation is

$$\left(\frac{\partial^2 C}{\partial X^2} + \frac{\partial^2 C}{\partial Y^2}\right) - V_X\frac{\partial C}{\partial X} = 0 \tag{3}$$

The boundary conditions for the latter partial differential equation are as follows:

$$\text{inlet:} \quad C = 1 \tag{4a}$$

(6) Henley, I. E.; Yunus, K.; Fisher, A. C. *J. Phys. Chem. B* **2003**, *107*, 3878–3884.

(7) (a) Richtmyer, R. D.; Morton, K. W. *Difference Methods for Initial-Value Problems*, 2nd ed.; John Wiley & Sons: New York, 1967. (b) Press, W. H.; Teukolsky, S. A.; Vetterling, W. T.; Flannery, B. P. *Numerical Recipes in C: The Art of Scientific Computing*, 2nd ed.; Cambridge University Press: Cambridge, U.K., 1992.

electrodes: $C = 0$ (4b)

other boundaries (insulator and outlet): $\frac{\partial C}{\partial \mathbf{n}} = 0$ (4c)

where **n** is the unit normal vector to the boundary.

Definition of the Flow Profile Function. We assume that the flow is described in the normalized terms by a function of the following class:

$$V_X(Y) = Pe\left(\frac{m+2}{2}\right)(1 - |2Y - 1|^{2/m}) \quad (5)$$

where m is the parameter that defines the level of "bluntness" of the flow profile ($0 < m \leq 1$). The interest of this formulation is that it encompasses all the classical shapes that may be achieved for the flow velocity profile within a channel. As particular cases, the function given as eq 5 describes the classical parabolic flow profile, which corresponds to $m = 1$, while $m \to 0$ describes the electro-osmotic flow. Furthermore, a simple addition of a constant term or a linear function of Y to the expression in eq 5 would allow treating the case of nonzero velocity at the channel walls. We will not consider this case in the following; therefore, we used the format given in eq 5. Figure 2 illustrates four sample flow profiles generated for different values of m while keeping the same Pe number (viz, the same volume flow rate and average flow velocity).

Equation 5 encompasses the case of electro-osmotic flows. However, because of the important electrical field that is required to create an electro-osmotic push, one experimentally cannot use any measurement based on electrochemical detection within the range where an effective electro-osmotic drive is active. Furthermore, would this be made possible, because an electro-osmotic flow $V_X(Y)$ is constant except within nanometric distances from the wall surfaces; a measurement of the average flow velocity is tantamount to determine $V_X(Y)$. This may be performed by a generator−collector system in a very simple manner.[3a]

However, in a real situation, even when the flow is driven electro-osmotically and this drive is interrupted over the channel range where an electrochemical detection is performed, it is

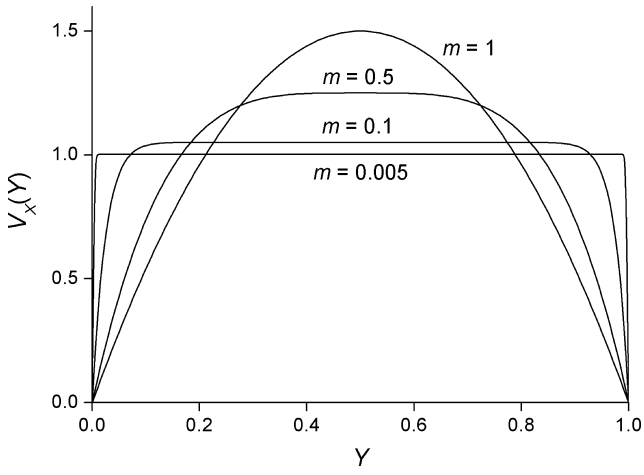

Figure 2. Effect of parameter m (values are shown on the curves) on the shape of the flow profile.

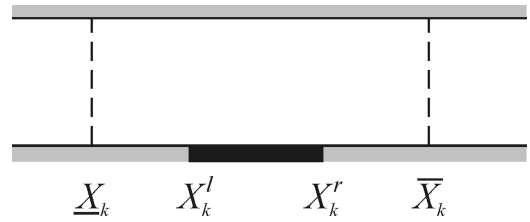

Figure 3. Schematic view of a single electrode compartment.

expected that viscosity will gradually transform the initially constant distribution of flow velocities into a parabolic one. Under such circumstances, it appears of interest to be able to assess the deformation of the initial electro-osmotic flow. In this respect, eq 5 provides an ideal view of such distorted flow, e.g., when $m \approx 0.5$. For this reason, in the following, we will address quantitatively the problem of flow reconstruction only for parabolic and distorted electro-osmotic cases, considering specifically the two following m values: $m = 1$ and 0.5. However, we will consider the case of pure electro-osmotic flow ($V_X(Y) =$ constant) in the section related to the optimization of the array geometry. Indeed, this will provide limiting cases between which any realistic flow should fall.

Evaluation of Theoretical Electrochemical Currents. The current flowing through the kth electrode may be computed using the classical definition:

$$i_k = nFDLc_0 \int_{X_k^l}^{X_k^r} \left(\frac{\partial C}{\partial Y}\right)_{Y=0} \mathrm{d}X \quad (6)$$

where n is the number of transferred electrons, F the Faraday constant, and L the length of band microelectrodes in the direction perpendicular to the flow (it is assumed to be equal to the channel width).

On the other hand, the value of the electrochemical current may be obtained from the mass conservation law. Indeed, consider an imaginary "electrode compartment", i.e., a fraction of the channel obtained by separating it from the rest of the solution volume by two cross sections perpendicular to the flow and located upstream and downstream of an electrode (see Figure 3) and *between* adjacent electrodes. At steady state, the amount of electroactive species reacting at the electrode surface in a unit of time is equal, by mass conservation, to the difference between the amount of this species that enters the compartment through its upstream boundary (corresponding to the vertical line with the abscissa $\underline{X}_k$ in Figure 3) and that which leaves the compartment through its downstream boundary (corresponding to the vertical line with the abscissa $\bar{X}_k$ in Figure 3). This fact can be formally stated as follows:

$$i_k = nFDLc_0 \int_0^1 [J_X(\underline{X}_k, Y) - J_X(\bar{X}_k, Y)] \, \mathrm{d}Y \quad (7)$$

where $J_X(X,Y) = -\partial C/\partial X + V_X C$ is the normalized flux. The latter expression is valid because of the fact that the electroactive species is not accumulated anywhere within the considered compartment and, at the same time, there are no sources of it therein. Thus, eq 7 is a direct equivalent of the Kirchhoff law of electrokinetics. Note also that the upstream and downstream boundaries of an electrode compartment can be located anywhere between adjacent electrodes.

Because of the fact that the two expressions for the evaluation of the current presented in eqs 6 and 7 are entirely equivalent, either of them may be used in the computations. However, since the described problem will be solved numerically (because analytical solution to it is not available in closed form), the two definitions will lead to different errors, because of the discretization properties of the numerical method. It has been found (see below) that a linear combination of the two expressions is best-suited for the numerical evaluation of the electrochemical current:

$$i_k = \frac{1}{2}nFDLc_0\left\{ \int_{X_k^l}^{X_k^r} \left(\frac{\partial C}{\partial Y}\right)_{Y=0} \mathrm{d}X + \int_0^1 [J_X(X_k, Y) - J_X(\bar{X}_k, Y)]\, \mathrm{d}Y \right\} \quad (8)$$

Flow Profile Determination (Inverse Problem). The ensemble of steady-state electrochemical currents recorded at a series of band microelectrodes operating in the generator mode carries the sought information about the flow profile shape through their nonlinear (and not available explicitly) dependence on the main flow parameters, viz, *Pe* and *m*. To extract this information, theoretical model currents must be fitted to experimental ones by varying these parameters (assuming that the actual flow profile in the experiment may be well described by a function of the form described by eq 5, which we will assume to be the case in the following). One possibility in this case consists of using the absolute values of the currents as given in the previous section. However, the evaluation of the absolute values of currents is dependent on precise knowledge of the values of all physicochemical parameters of the system, including the diffusion coefficient of the electroactive species and its bulk concentration at the channel inlet. The latter may be difficult to control exactly, especially when the channel section under scrutiny is a part of a complicated microfluidic device in which some adsorption may have occurred before the flow measurement stage examined here. However, eq 8 shows that c_0 is simply an amplifying factor that affects the currents of all the electrodes of the array in the same way. Thus, the consideration of *relative* currents seems to be a remedy that allows the profile determination procedure to be freed from unnecessary parameters.

The goal of fitting experimental and theoretical currents is to achieve the minimum of the following least-squares functional:

$$\Phi(\mathbf{p}) = \frac{1}{N_{\mathrm{el}} - 1} \sum_{k=2}^{N_{\mathrm{el}}} \left(\frac{i_k(\mathbf{p})}{i_1(\mathbf{p})} \times \frac{i_1^{\mathrm{exp}}}{i_k^{\mathrm{exp}}} - 1 \right)^2 \quad (9)$$

where $\mathbf{p}$ is the vector of flow profile parameters (i.e., it consists of the values of *Pe* and *m*), $i_k(\mathbf{p})$ the theoretically computed value of current at the *k*th electrode for the parameter vector $\mathbf{p}$, and i_k^{exp} the value of the experimental current at the same electrode.

OPTIMIZATION OF ELECTRODE ARRAY LAYOUT

As in our previous works,[4] we wish to examine the influence of the electrode layout and flow intensity on the outcome of the flow determination procedure. It was established that the quality of fitting experimental data is strongly dependent on the average flow velocity, so that it is expected to be sensitive to the flow profile shape when neither diffusion nor convection plays the dominant role in mass transport. Thus, it was postulated that an electrode should "feel" at least through one-third of the channel height; specifically, the diffusion layer extending vertically directly above the electrode should be at least of thickness $h/3$.

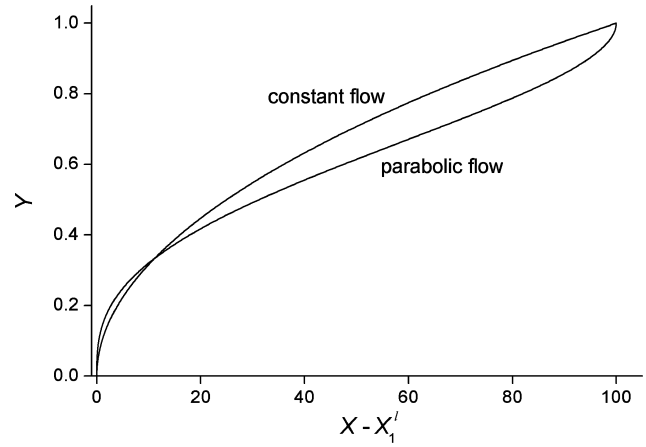

Figure 4. Particle trajectories for the constant and parabolic flows corresponding to $Pe = 100$.

In this work, we will proceed along similar lines to optimize the mutual placement and widths of electrodes forming a sensing array. It will be assumed that the entire array should be of sufficient width for the diffusion layer created by all the electrodes together to extend into the flowing solution up to the channel ceiling, i.e., the diffusion layer should extend up to $y = h$ while the solution flows over the electrode array. We will consider the cases of electro-osmotic and parabolic flows separately, because they represent the two experimentally most frequently encountered cases.

Parabolic Flow. Let us consider a normalized flow profile given by a function $V_X(Y)$ and assume that the flow is sufficiently fast. The latter assumption allows us to ignore, in the following derivations, the diffusional component in the displacement of molecules in the direction of the flow. Consider then a particle released at normalized time $\tau = Dt/h^2 = 0$ from the point $X = X_1^l$, $Y = 0$ (i.e., from the upstream edge of the first electrode), which moves diffusionally in the vertical direction and is carried by the convective flow in the axial direction. Its trajectory is described by the following pair of equations:

$$Y(\tau) = \sqrt{\tau}$$
$$X(\tau) - X_1^l = \int_0^\tau V_X(Y(\tau))\, \mathrm{d}\tau \quad (10)$$

The formulation of eq 10 does not require a precise expression for $V_X(Y)$; therefore, any such function may be used to find a trajectory. For instance, Figure 4 shows trajectories of molecules for the parabolic and constant (electro-osmotic) flows.

Let us now consider the classical parabolic flow profile, given by

$$V_X(Y) = 6Pe(Y - Y^2) \quad (11)$$

Assuming that the overall diffusion layer of the array extends up to the ceiling of the channel (i.e., in dimensionless terms, this

diffusion layer thickness is $\eta_{max} = (\tau_{max})^{1/2} = 1$), we obtain the following expression for the dimensionless array width W_{array}:

$$W_{array} = X^r_{N_{el}} - X^l_1 = N_{el}W + \sum_{i=1}^{N_{el}-1} G_i = 6Pe \times \int_0^{\tau_{max}=1} (\sqrt{\tau} - \tau)\, d\tau = Pe \quad (12)$$

where W is the dimensionless electrode width and G_i is the dimensionless width of the ith gap.

The detection of the flow profile by an array of band microelectrodes may be viewed as a progressive collection of the electroactive species from different layers of the solution, when each subsequent electrode probes the concentration distribution deeper into the solution, which has been convoluted with the disturbances enforced by any upstream electrodes. Under such conditions, it seems that each electrode probing the same fraction of the channel height would give the best sensitivity toward the flow velocity distribution along the vertical axis.

To fulfill this requirement, each electrode should probe a fraction of the channel height of (normalized) thickness $1/N_{el}$. Hence, the maximum height to be probed by the kth electrode is

$$\eta_k = \sqrt{\tau_k} = \frac{k}{N_{el}} \quad (13)$$

and then

$$kW + \sum_{i=1}^{k-1} G_i = Pe\left[4\left(\frac{k}{N_{el}}\right)^3 - 3\left(\frac{k}{N_{el}}\right)^4\right] \quad (14)$$

from which one may obtain the following expressions for gap sizes:

$$G_1 = Pe\left[4\left(\frac{2}{N_{el}}\right)^3 - 3\left(\frac{2}{N_{el}}\right)^4\right] - 2W \quad (15a)$$

$$G_s = Pe\left\{\left[4\left(\frac{s+1}{N_{el}}\right)^3 - 3\left(\frac{s+1}{N_{el}}\right)^4\right] - \left[4\left(\frac{s}{N_{el}}\right)^3 - 3\left(\frac{s}{N_{el}}\right)^4\right]\right\} - W \quad (\text{for } s = 2, ..., N_{el} - 1) \quad (15b)$$

Note that the above expressions will ensure exactly equal conditions for each of the electrodes if the dimensionless electrode width W satisfies the following relation:

$$W = Pe\left(\frac{4N_{el} - 1}{N_{el}^4}\right) \quad (16)$$

so that the first electrode of the array probes exactly $1/N_{el}$ of the channel height.

Electro-osmotic Flow. Using the general expressions described in eq 10 from the previous section, with a constant flow profile $V_X(Y) \equiv Pe$, we arrive at the following condition for the overall band microelectrode array width corresponding to a diffusion layer of thickness h:

$$W_{array} = \int_0^{\tau_{max}=1} Pe\, d\tau = Pe \quad (17)$$

For the electrodes of the array to probe the same thickness layers of the flowing solution, they must be separated by gaps whose sizes are dictated by the following expressions:

$$G_1 = Pe\left(\frac{4}{N_{el}^2}\right) - 2W \quad (18a)$$

$$G_s = Pe\left(\frac{2s+1}{N_{el}^2}\right) - W \qquad (s = 2, ..., N_{el} - 1) \quad (18b)$$

so that the gap sizes increase as an arithmetic progression.

Also, as in the case of a parabolic flow, the first electrode will probe the same fraction of the channel height as the others if their widths satisfy the following relation:

$$W = \frac{Pe}{N_{el}^2} \quad (19)$$

NUMERICAL SIMULATION

Solution of the Diffusion-Convection Problem (Direct Problem). Because the diffusion−convection problem is considered under steady-state conditions, special care must be taken of singularities at upstream and downstream edges of band microelectrodes. To enhance the numerical grid resolution around the edges of the electrodes, coordinate transformations were used in both the X- and Y-directions. The nonuniform grid in the X-direction was constructed using Bezier splines over each electrode and gap. A Bezier spline defining the mapping of X into a transformed coordinate ξ was constructed using the expressions

$$X(s) = 3q_{11}s(1 - s)^2 + 3q_{21}s^2(1 - s) + s^3 \quad (20a)$$

and

$$\xi(s) = 3q_{12}s(1 - s)^2 + 3q_{22}s^2(1 - s) + s^3 \quad (20b)$$

where q_{11}, q_{12}, q_{21}, and q_{22} are spline parameters and $0 \le s \le 1$ is a dummy variable (see Figure 5). Next, the interval [0, 1] of the variation of $\xi(s)$ was divided into NX equal steps and the corresponding X-points were found by the inversion of the spline yielding the required nonuniform node distribution in the X-direction. The density of nodes in the obtained grid is highest around electrode edges and gradually decreases between them.

Figure 5a shows the coordinate transformation over the electrode, which was observed to give highly accurate results. Note that the ensuing grid compression is higher at the upstream edge of the electrode, which is conditioned by higher concentration gradients (and, hence, flux) in this area (see Figure 5b). The interest of such coordinate transformation along the X-direction is readily evidenced by the smoothness of the flux over the transformed electrode in Figure 5c.

The grid in the Y-direction was also compressed near the floor and ceiling of the channel. This was required, because of either high concentration gradients near the electrode surfaces or diffusion dominating over convection in the boundary layer at the

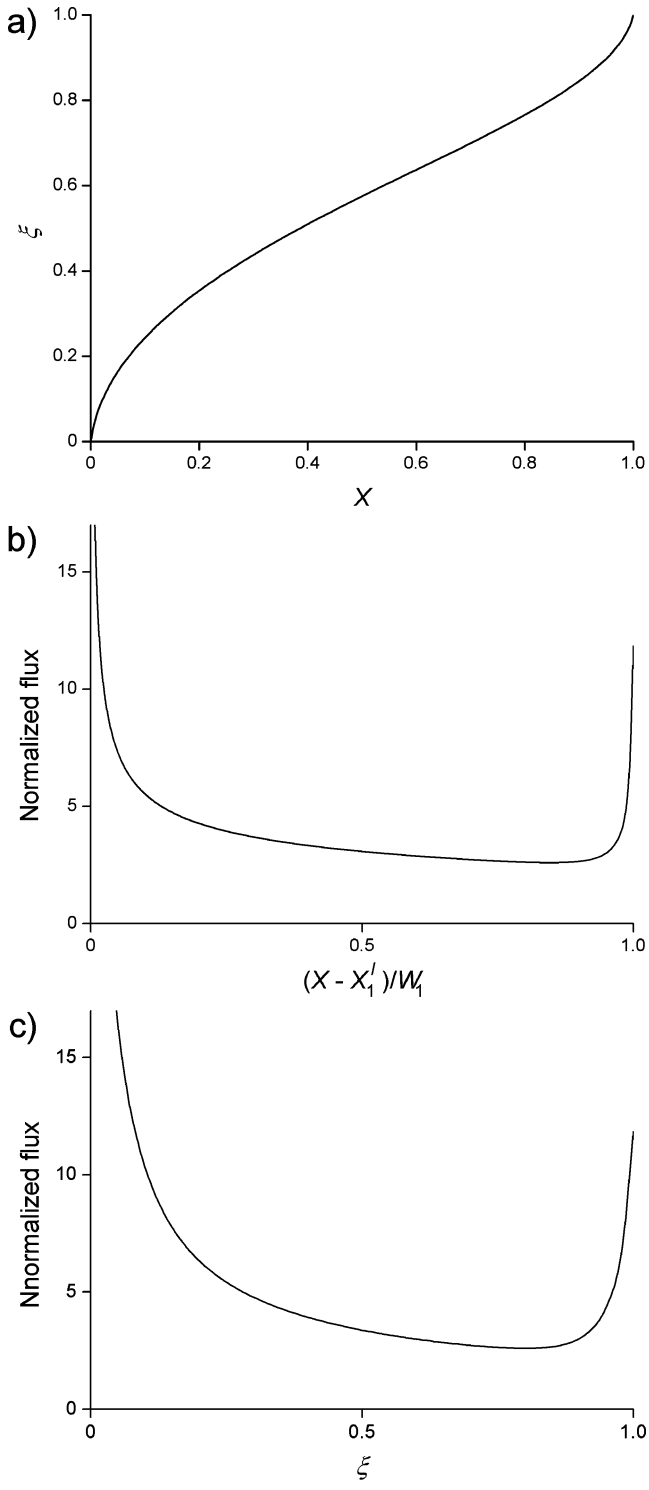

Figure 5. (a) Coordinate transformation in the X coordinate over an electrode. Parameter values: $q_{11} = 0.05$, $q_{12} = 0.5$, $q_{21} = 0.95$, $q_{22} = 0.7$. (b) Normalized current density over the first electrode, indicating flux singularities at its ends. (c) Normalized current density plotted versus ξ and showing smoothed variations of the flux.

channel ceiling. The transformation is shown in Figure 6, together with the Bezier spline parameters.

The overall nonuniform grid obtained in this fashion was used for the discretization of the boundary value problem described by eqs 3 and eqs 4a−4c, using upwind discretization of the convection term and the Alternating Direction Implicit (ADI) method[7a] for the solution of the corresponding pseudo-transient

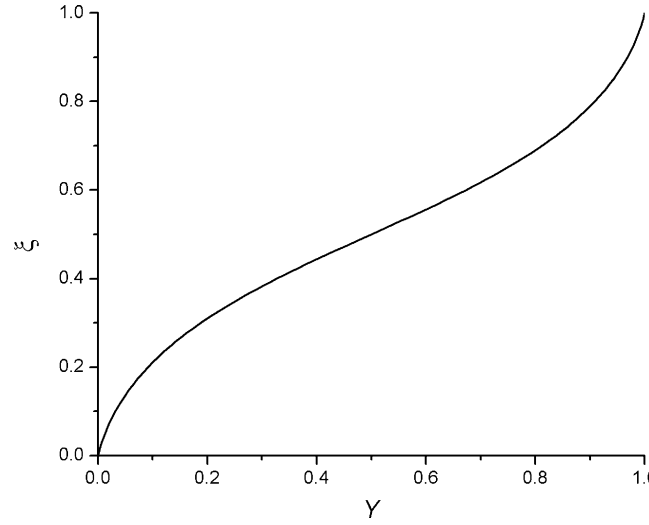

Figure 6. Coordinate transformation in the Y-coordinate. Parameter values: $q_{11} = 0.1$, $q_{12} = 0.5$, $q_{21} = 0.9$, and $q_{22} = 0.5$.

problem (i.e., the original steady-state problem was solved by introducing a fake time variable θ and solving the resulting equation $\partial C/\partial\theta = \Delta C - V_X\, \partial C/\partial X$ with increasing θ until steady state was reached, that is, until $\partial C/\partial\theta$ became sufficiently small). Splitting the solution along the X- and Y-directions in the ADI method implies that each iteration of the method consists in the solution of $NX + NY$ tridiagonal linear systems.

Solution of the Fitting Problem (Inverse Problem). Minimization of the functional described by eq 9 is achieved by numerical minimization methods that involve solution of the direct problem (computing the concentration distribution and electrochemical currents) at every iteration. The efficiency of the minimization of the functional described by eq 9 is dependent on the available amount of information about it. In the case when only the functional values may be computed for a given set of parameters, the minimization of the functional may be performed using zero-order minimization methods (such as, e.g., the Nelder−Mead method[7b]), which generally require a large number of functional evaluations for convergence. To improve computational efficiency, the Nelder−Mead method was combined with a direct search approach to determine a good initial point for further minimization.

Computational Details. The simulation approaches for the solution of the direct and inverse diffusion−convection problems were implemented in a computer program written in Borland Delphi 7 programming environment and executed on a personal computer (PC) that was equipped with an Intel Pentium D processor (2.8 GHz, 512MB of RAM).

Numerical experiments revealed that, for an electrode array with $W_i = G_i = 1$ (i.e., all electrodes and gaps of the same size), a grid with 100 nodes in the Y-direction and 100 nodes per each electrode or gap was sufficient to achieve an accuracy of better than 0.7% for moderately fast flows ($Pe < 100$). For optimized arrays, gap widths are dependent on the number of electrodes in the array, as well as on the prevailing Pe number, according to eqs 15a, 15b, and 16 or eqs 18a, 18b, and 19. Therefore, to keep approximately the same grid density on both sides of each electrode edge, and, at the same time, reduce the overall number of grid points in the X-direction, the following

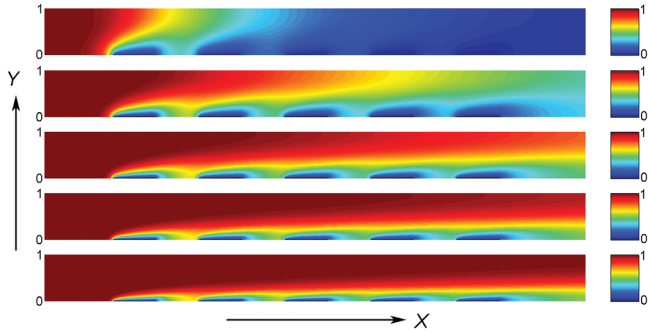

Figure 7. Normalized concentration (see color-coded scale in the right panels) distributions for $m = 1$ and different Pe numbers: $Pe =$ 5, 20, 50, 100, and 200 (from top to bottom).

approach was used. The number of nodes corresponding to each electrode (all of them being of the same normalized width W) was set to be 100, whereas the number of nodes for each kth gap was calculated using the expression $100(G_k/W)^{3/4}$.

RESULTS AND DISCUSSION

The efficiency of the flow determination procedure was tested by running a series of simulations with different flow profiles and rates to obtain dummy experimental (pseudo-experimental) data, which were then introduced into the fitting program as input. For the reasons previously detailed, we will consider only parabolic flows ($m = 1$) and exemplify the method validity for distorted electro-osmotic flows by detailing the results for $m = 0.5$.

To test the fit quality, the following factor is introduced:

$$\rho = \frac{1}{Pe^{\text{exp}}} \int_0^1 |V_X^*(Y) - V_X^{\text{exp}}(Y)|\, dY \qquad (21)$$

where $V_X^{\text{exp}}(Y)$ is the flow profile used to compute pseudo-experimental currents, Pe^{exp} the corresponding Peclet number, and $V_X^*(Y)$ is the flow profile function resulting from the minimization of the functional described by eq 9. Such a definition of the fit quality factor ensures that the comparison is focused on the evaluation of the shape of the flow profile resulting from the fitting, because of the normalization with respect to Pe^{exp}, thus providing a fair comparison of the results.

Figure 7 shows concentration distributions computed for $m = 1$ and five different Pe values for an electrode array with fixed widths of all electrodes and gaps: $W = G_k = 1$, $k = 1$, ..., 4. Figure 7 shows that, for Pe values that are too low (the top case in Figure 7), the first electrode probes almost the entire channel, with the residual section being fully tested by the second one, so that the expected precision is low. Indeed, the following electrodes do not contribute to the reconstruction procedure. Conversely, when Pe is too large (the bottom two cases in Figure 7), the entire array probes too small a fraction of the channel, so high precision is obtained for the flow velocities near the channel floor but poor accuracy is obtained on the total flux reconstruction. Hence, for a given electrode placement and widths, there is an optimal range of Pe values over which the flow velocity can be reconstructed with both good precision and good accuracy. This was expressed analytically by the optimization rules given in eqs eqs 15a, 15b, and 16 or eqs 18a, 18b, and 19, but Figure 7 shows it in a form that graphically exemplifies the very reason for these optimization conditions.

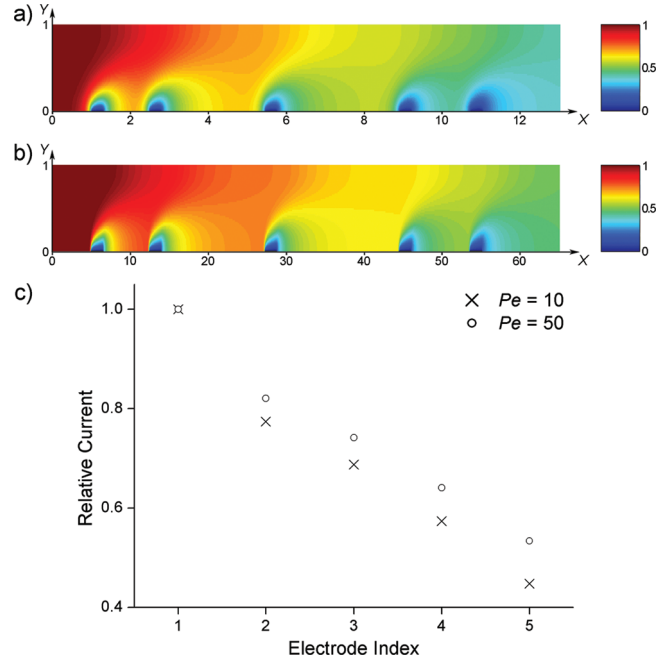

Figure 8. (a, b) Normalized concentration distributions (see Figure 7 for presentation) and (c) relative currents for the case $m = 1$ (parabolic flow), $N_{el} = 5$ (Pe =10 in panel a and $Pe = 50$ in panel b). Optimal electrode and gap widths are given in Table 1.

The gap and electrode width optimization approach developed above allows for the creation of equal conditions for each electrode in the array under various flow conditions. This is illustrated in Figures 8a and 8b, which show computed concentration distributions for two different electrode arrays consisting of five electrodes optimized for best performance under parabolic flows with $Pe = 10$ and $Pe = 50$. Electrode widths W (the same for all electrodes in each array) and gaps sizes were calculated using expressions 15a,15b, and 16, and their values are given in Table 1. Note that the concentration distributions shown in Figures 8a and 8b are very similar (although the X scales are different), which proves that, in each case, the electrodes perform under optimal conditions, because of their correct sizes and mutual location (see Figure 7 for comparison, where all electrodes and gaps were the same width). This is further exemplified in Figure 8c, which shows the relative currents (i_k/i_1) computed for the band microelectrode arrays and flow conditions, as shown in Figures 8a and 8b, respectively. The currents decay almost linearly with the electrode index (except the second electrode current), which implies that all electrodes consume approximately equal amounts of the electroactive species (viz, the average concentration in the vertical cross section of the channel reduces by roughly the same amount after each electrode). With increasing Pe, each electrode is able to "catch" a gradually smaller fraction of material flowing past the electrode. Hence, the fraction consumed by the first electrode also is reduced, which results in an increase in the relative currents of electrodes with indices 2, 3, ...

Table 1. Fitting Results for Optimal Band Microelectrode Arrays ($m = 1$, Parabolic Profiles)

Pe	W	G_1	G_2	G_3	G_4	ρ	$\Phi(\mathbf{p}^*)$
				$N_{el} = 3$			
10	1.358	3.210	2.716			2.156×10^{-3}	3.832×10^{-10}
20	2.716	6.420	5.432			7.053×10^{-2}	2.551×10^{-7}
30	4.074	9.630	8.148			9.433×10^{-2}	4.804×10^{-7}
40	5.432	12.840	10.864			1.108×10^{-1}	6.558×10^{-7}
50	6.790	16.049	13.580			1.329×10^{-1}	1.122×10^{-6}
				$N_{el} = 4$			
10	0.586	1.953	3.672	2.031		2.999×10^{-5}	2.405×10^{-10}
20	1.172	3.906	7.344	4.063		3.050×10^{-3}	1.368×10^{-6}
30	1.758	5.859	11.016	6.094		$<10^{-8}$	3.077×10^{-14}
40	2.344	7.813	14.688	8.125		2.500×10^{-5}	3.918×10^{-11}
50	2.930	9.766	18.359	10.156		1.300×10^{-3}	1.192×10^{-7}
				$N_{el} = 5$			
10	0.304	1.184	2.656	3.136	1.504	2.999×10^{-5}	1.313×10^{-10}
20	0.608	2.368	5.312	6.272	3.008	1.116×10^{-4}	6.181×10^{-11}
30	0.912	3.552	7.968	9.408	4.512	$<10^{-8}$	1.885×10^{-13}
40	1.216	4.736	10.624	12.544	6.016	8.300×10^{-4}	5.139×10^{-11}
50	1.520	5.920	13.280	15.680	7.520	$<10^{-8}$	5.495×10^{-13}

Figure 9 illustrates the same analysis for a distorted electro-osmotic flow (viz., $m = 0.5$) probed by an array of five electrodes with optimized gaps distribution (eqs 15a, 15b, and 16) derived for parabolic profiles. Because this flow profile is not drastically different from the parabolic profile (see Figure 2), the concentration distributions are reminiscent of those in Figure 8a and 8b, although relative electrochemical currents in Figure 9c differ by 3%−6.5% from those for purely parabolic profiles in Figure 8c.

The flow profile determination procedure was performed for a range of flow rates (viz, Pe values) and two values of m corresponding to the parabolic flow ($m = 1$) and distorted electro-osmotic flow ($m = 0.5$) for optimum band microelectrode arrays, as determined by eqs 15a, 15b, and 16. For this study, we used arrays of 3−5 electrodes. Indeed, when fitting relative currents (viz, minimizing the functional described by eq 9), the number of known quantities is $N_{el} - 1$, because the relative current of the first electrode is always 1. Because of the fact that the number of unknowns is 2 (Pe and m), the number of experimental relative currents ($N_{el} - 1$) must be at least 2; hence, $N_{el} \geq 3$. The fitting was performed for a range of Pe values of 10−50. This choice is related to the expected experimental range of flow intensity[3] and also corresponds to the intermediate flow regimes when neither diffusion nor convection is a dominant factor of mass transport. The latter ensures that the electrochemical currents recorded at the electrodes of the array are sufficiently sensitive to the flow profile shape.[4]

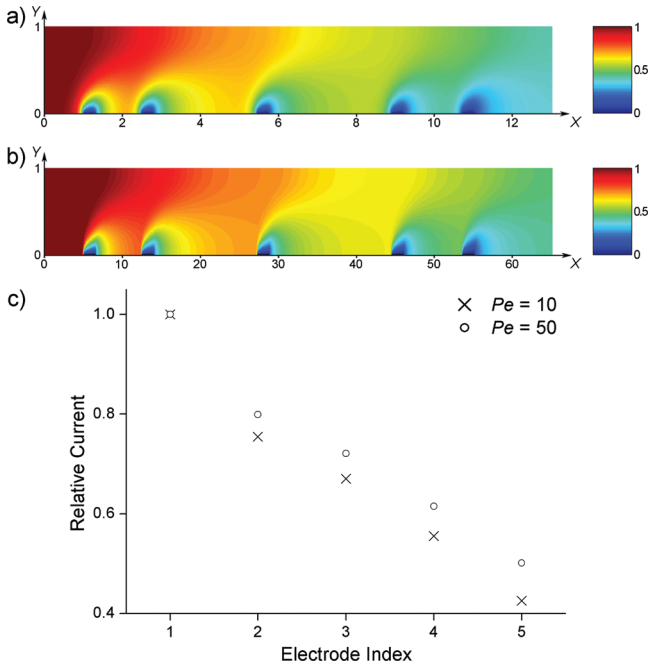

Figure 9. (a, b) Normalized concentration distributions (see Figure 7 for presentation) for $m = 0.5$ (distorted electro-osmotic flows), $N_{el} = 5$ ($Pe = 10$ in panel a and $Pe = 50$ in panel b) and (c) relative currents for the same Pe values. Electrode and gap widths were optimized for parabolic profiles.

Table 2. Fitting Results for Band Microelectrode Arrays Optimized for Parabolic Profiles and Employed to Reconstruct Distorted Electroosmotic Flow Profiles ($m = 0.5$)

Pe	W	G_1	G_2	G_3	G_4	ρ	$\Phi(\mathbf{p}^*)$
				$N_{el} = 3$			
10	1.358	3.210	2.716			6.111×10^{-2}	3.063×10^{-6}
20	2.716	6.420	5.432			7.382×10^{-3}	8.462×10^{-9}
30	4.074	9.630	8.148			5.751×10^{-2}	6.275×10^{-7}
40	5.432	12.840	10.864			1.328×10^{-2}	2.189×10^{-8}
50	6.790	16.049	13.580			2.105×10^{-1}	1.244×10^{-6}
				$N_{el} = 4$			
10	0.586	1.953	3.672	2.031		2.274×10^{-4}	2.934×10^{-10}
20	1.172	3.906	7.344	4.063		1.387×10^{-4}	1.416×10^{-10}
30	1.758	5.859	11.016	6.094		$<10^{-8}$	9.693×10^{-14}
40	2.344	7.813	14.688	8.125		5.585×10^{-3}	3.865×10^{-8}
50	2.930	9.766	18.359	10.156		1.148×10^{-5}	4.421×10^{-12}
				$N_{el} = 5$			
10	0.304	1.184	2.656	3.136	1.504	1.062×10^{-4}	7.047×10^{-11}
20	0.608	2.368	5.312	6.272	3.008	2.678×10^{-5}	2.452×10^{-11}
30	0.912	3.552	7.968	9.408	4.512	$<10^{-8}$	5.203×10^{-13}
40	1.216	4.736	10.624	12.544	6.016	7.500×10^{-5}	2.569×10^{-11}
50	1.520	5.920	13.280	15.680	7.520	2.000×10^{-5}	4.231×10^{-12}

Tables 1 and 2 respectively contain the results of fitting for different values of N_{el} and Pe for the parabolic flow profile ($m = 1$) and distorted electro-osmotic flow profile (viz, contaminated by parabolic friction near the walls, $m = 0.5$). Tables 1 and 2 also provide values of normalized electrode widths and gap sizes obtained for the respective values of N_{el} and Pe using eqs 15a and 16. The outcome of fitting (performed using a computer program implementing the developed approach; see the "Numerical Simulation" section) in each case is characterized by the minimized value of the functional $\Phi(\mathbf{p}^*)$ (where $\mathbf{p}^*$ is the vector of flow parameters providing the best fit) and the value of the fit quality factor ρ.

The results presented in Tables 1 and 2 and Figure 10 clearly demonstrate that the flow determination can be successfully performed for any Pe value in the aforementioned range, using an array of 4 or more band microelectrodes. On the other hand, the values of the fitting quality factor are, in most cases, significantly poorer for $N_{el} = 3$, indicating that steady-state currents for a three-electrode device (viz, two independent relative currents) do not provide a sufficient amount of information for the determination of the actual flow profile, except maybe at the lowest values of Pe.

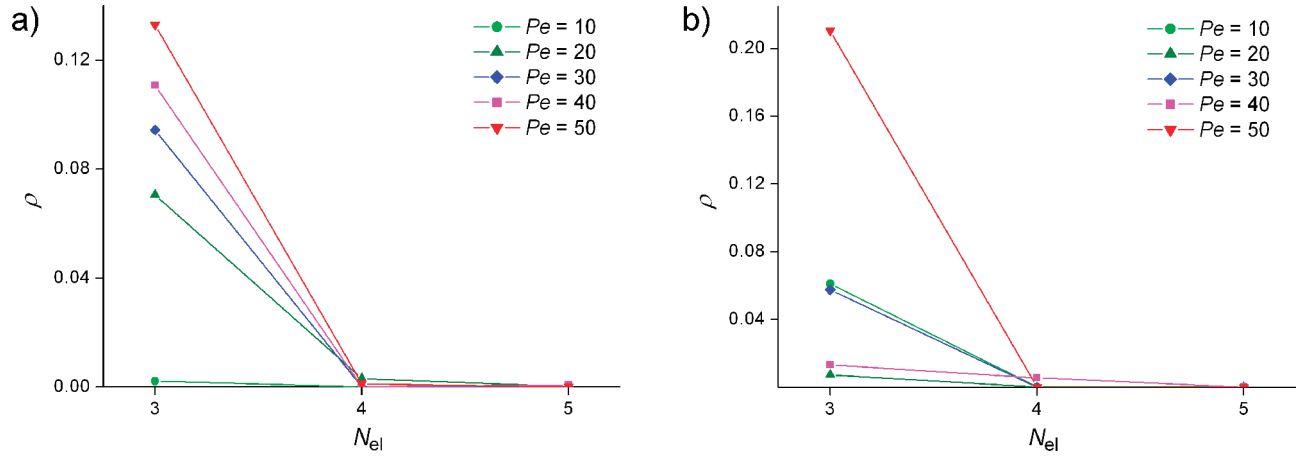

Figure 10. Dependence of the fit quality factor (ρ) on the number of electrodes in the array (N_{el}) for (a) parabolic profiles ($m = 1$) and (b) distorted electro-osmotic profiles ($m = 0.5$) for different Pe values (see Tables 1 and 2).

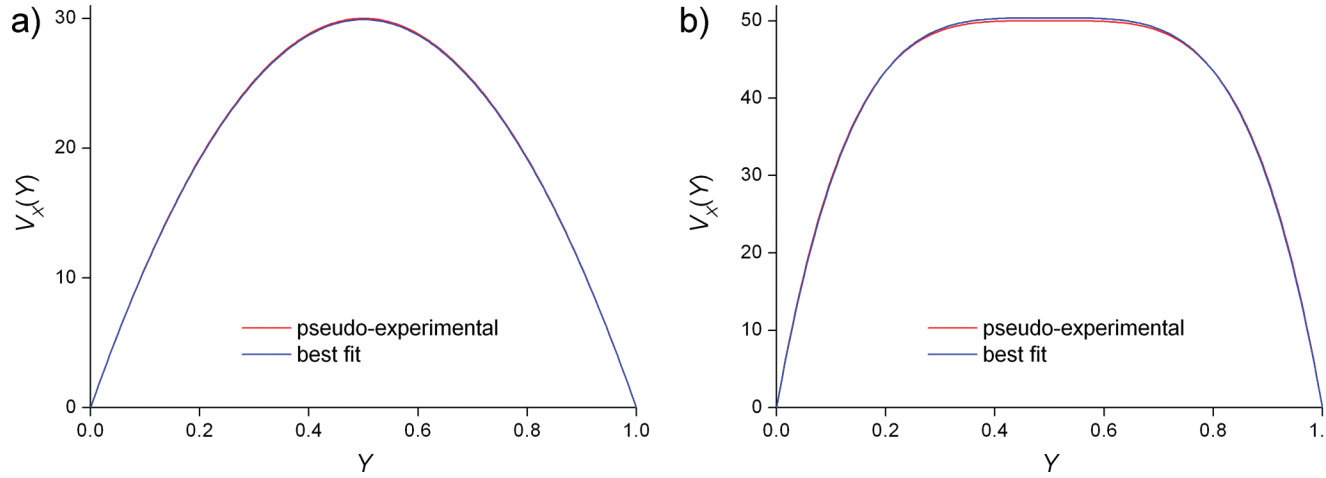

Figure 11. Correspondence between pseudo-experimental and best-fit flow profiles for $N_{el} = 4$ and (a) $Pe = 20$, $m = 1$ and (b) $Pe = 40$, $m = 0.5$ (see Tables 1 and 2).

Figure 11 demonstrates the agreement between flow profiles that were used to compute pseudo-experimental current data and those obtained after fitting for two cases detailed in Tables 1 and 2 based on the relative steady-state currents. These data correspond to the worst cases of fitting (viz, corresponding to largest values of ρ) among those for $N_{el} = 4$. The excellent agreement in both cases indicates the high quality of fitting results for $N_{el} = 4$ and $N_{el} = 5$, because the correspondence between flow profiles is even better in other cases. The corresponding pseudo-experimental and best-fit currents are not visualized here, because they appear to be indistinguishable.

CONCLUSIONS

In this work, the possibility of reconstructing the flow velocity profile developed within a microfluidic channel on the basis of absolute or relative steady-state electrochemical currents measured at an array of N_{el} band microelectrodes has been investigated theoretically. The method has been demonstrated to give excellent results, provided the arrays consist of a sufficient number of electrodes.

When using the general flow velocity expression (eq 5), reconstructing the distribution of velocities requires two parameters, viz, $Pe = v_{avg}h/D$ which relates the average flow velocity to the channel height and the diffusion coefficient of the electroactive probe, and a shape factor m, so that $N_{el} = 3$ or $N_{el} = 4$, respectively, for absolute current or relative current measurements, are sufficient to provide excellent reconstruction. If a more complicated flow velocity equation were to be used, e.g., one requiring the determination of p parameters, these numbers would be $N_{el} = p + 1$ or $N_{el} = p + 2$, respectively.

The method is based on introducing a competition between convective and diffusionnal transports. It then requires that (i) each electrode of the array develops a diffusion layer extending over a significant fraction of the channel height, to probe the entire channel collectively, and (ii) the gaps that separate these electrodes are of sufficient size to allow diffusion to re-feed the solution volume exhausted by each electrode before the next one operates, although not too large, to avoid a statistical homogenization of the redox probe concentration across the channel height. This double geometrical constraint may be taken into account to define the optimal geometry of the reporting band electrode array for any set of Pe and N_{el} values, provided that N_{el} respects the aforementioned relationships. Interestingly, these optimal configurations impose that the gap size increases along the

array to account for the progressive weakening of diffusion gradients while deeper and deeper zones of the channel are probed. Although the optimal geometry provides the most spectacular results, the method performs excellently when the *Pe* value departs from the value used to define the most advantageous configuration as soon as the aforementioned constraints (see above points i and ii) are qualitatively respected. This ensures that good performances are expected over a rather broad range of *Pe* values around that for which the array was configured. Because a microchannel is generally designed for performing within a specific range of v_{avg} values, this requirement does not constitute a limitation for the method.

ACKNOWLEDGMENT

This work was partially supported by the CNRS (UMR 8640 "PASTEUR"), Ecole Normale Superieure (ENS), University Pierre and Marie Curie (UPMC), and the French Ministry of Research. In Kharkov, this work was supported by the Ministry of Education and Science of Ukraine (Project No. M/71-2009).

Received for review May 18, 2009. Accepted August 1, 2009.

AC9010827